Additional characterization of Dome-C to improve its use as an invariant visible calibration target

David R. Doelling*[a],Rajendra Bhatt[b], Benjamin R. Scarino[b], Arun Gopalan[b], David Rutan[b], Ryan Scott[b], Conor O. Haney[b]

[a] NASA Langley Research Center, 21 Langley Blvd MS 420, Hampton, VA 23681-2199 USA

[b] SSAI, One Enterprise Pkwy Ste 200, Hampton, VA 23666 USA

*david.r.doelling@nasa.gov; phone 1 (757) 864-2155

ABSTRACT

Dome-C is a recommended CEOS invariant target that has been utilized by the calibration community for several decades for monitoring onboard sensor calibration systems as well radiometric inter-comparisons. Dome-C is a high-altitude Earth target located on the East Antarctic interior plateau, which has a permanent bright, flat, and homogeneous snow-covered surface with little aerosol, cloud cover, snowfall, and water vapor burden. This paper describes angular directional models for characterizing the Dome-C top-of-atmosphere (TOA) radiances as a function of cosine solar zenith angle for pre-solstice and post-solstice conditions. The 0.86-µm channel Dome-C reflectance decreases over the summer due to snow metamorphosis is not observed by the visible channels. Coinciding Terra and Aqua MODIS Dome-C reflectance showed occasional inter-annual anomalies when compared against the deep convective cloud and Libya-4 invariant targets observations. Further characterization of the Dome-C reflectances with the Dome-C surface broadband albedo, Antarctic Oscillation (AAO) index, and ozone concentration values were evaluated. A strong correlation with ozone was found for the 0.55-µm and 0.65-µm MODIS channels. The monthly Dome-C reflectances were linearly regressed with ozone to derive the ozone correction coefficients. The uncertainty in the Aqua- and Terra-MODIS Dome-C trends was reduced by half after applying ozone corrections to both the 0.55-µm and 0.65-µm channel TOA observations.

Keywords: MODIS visible band calibration stability, Dome Concordia invariant target calibration, visible band ozone absorption

1. INTRODUCTION

The NASA Clouds and the Earth's Radiant Energy System (CERES) [1] project uses Dome Concordia (Dome-C) as an invariant target to independently monitor the radiometric stability of Moderate Resolution Imaging Spectroradiometer (MODIS) and Visible Infrared Imaging Radiometer Suite (VIIRS) L1B imager reflective solar band (RSB) channel reflectances. CERES also uses deep convective clouds (DCC) and the Libya-4 desert target to monitor the stability of these imagers. The MODIS and VIIRS sensors have onboard calibration systems that reliably correct for any optical degradation. For real-time processing, the VIIRS characterization support team (VCST) updates the calibration coefficients if the onboard calibration systems indicate that the optical throughput has varied by more than 0.2% [Jack Xiong personal communication]. This forward processing procedure might allow small long-term drifts to go undetected. The CERES and VIIRS product versioning and reprocessing efforts are not coordinated. If the CERES project finds a need to reprocess the record to preserve the climate quality due to unforeseen circumstances, such as satellite outages or other input dataset algorithm changes, the CERES project can mitigate the imager channel drifts before reprocessing based on the invariant target radiometric stability analysis. However, such calibration drifts are corrected by the VCST when an updated VIIRS L1B dataset collection is released. CERES relies on MODIS and VIIRS cloud properties to convert the CERES observed radiances into fluxes. The radiance to flux conversion models are based on cloud properties obtained from the early CERES record. Any change in the cloud properties due to imager calibration drifts could impact the resulting fluxes [2]. Also, the geostationary imager radiances, which are used to determine the regional diurnal flux signal in between Aqua and Terra measurements, are radiometrically scaled to Aqua-MODIS to facilitate consistent cloud and fluxes [3].

The CERES project monitors the imager RSB channels in near real-time. Any unidentified reflectance variability in the invariant target could bias the monitoring results. By using DCC, Libya-4 and Dome-C invariant targets, any one invariant target reflectance outlier not observed by the other two targets would suggest that the outlier should not be considered when monitoring the invariant target. However, this approach only identifies large anomalies, since the invariant targets are not completely unvarying. The three independent invariant target anomalies are not correlated with global scale weather events except for large volcanic eruptions. This approach is not able to identify small scale invariant target anomalies with respect to the other two targets, which are also varying in both time and magnitude. Another approach would be to further characterize the Dome-C invariant target by using real-time auxiliary data that can be correlated with the Dome-C reflectances. Currently, the Dome-C invariant target methodology only accounts for angular dependencies. The Dome-C monitoring methodology is only effective for RSB with wavelengths less than 1 µm. For wavelengths greater than 1 µm the signal to noise is reduced due to the limited radiance values, which are a result of the lower surface reflectivity in combination with the large solar zenith angles. Figure 1 shows the SCanning Imaging Absorption SpectroMeter for Atmospheric CHartographY (SCIAMACHY) hyper-spectral mean radiance (blue points) and standard deviation (gray points) observed over Dome-C. Note the radiance standard deviation is similar to the mean due to the quickly changing solar illumination conditions observed over the Dome-C summer.

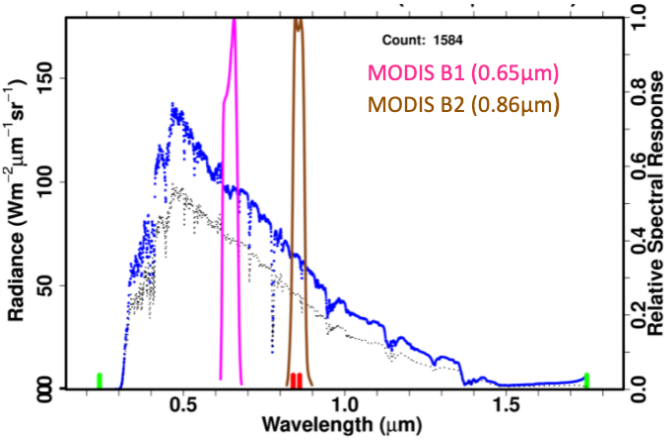

Fig. 1. The Dome-C SCIAMACHY mean (blue dots) and standard deviation (gray dots) spectral radiances observed between 2002 and 2010. The large standard deviation is due to large range of solar zenith angles observed between during the Dome-C austral summer, which are never less than 60°. For reference, the MODIS band 1 and 2 normalized spectral response functions are also shown. Note the for wavelengths greater than 1 µm, the radiance is much smaller than for visible wavelengths.

Polar ice pseudo invariant calibration sites (PICS) have been used to calibrate satellite sensors vicariously for over two decades. Beginning in the 1980's, the International Satellite Cloud Climatology Project (ISCCP) project used the clear-sky portion of the Earth as an invariant target, which included Antarctica to track the degradation of the NOAA Advanced Very High-Resolution Radiometer (AVHRR) imagers [4]. By the 1990's, the use of bright desert invariant targets was used to officially derive the AVHRR sensor calibration coefficients [5][6][7]. However, certain limitations of desert targets were realized, which included identifying aerosols, dust, and cloud events as well as accounting for surface bidirectional and humidity effects. By the late 1990's, the Antarctic plateau was recognized as having a stable surface reflectivity over a large region of interest with an extremely dry atmosphere with few aerosols and clouds. Loeb et al. 1997 [8] characterized the Antarctic TOA reflectance by a 2nd order regression with cosine of the solar zenith angle utilizing spatially uniform observations. Masonis et al. 2001 [9] utilized an empirical derived BRDF model and TOMS ozone measurements over Antarctica to determine the AVHRR calibration coefficients. Updated Antarctic based AVHRR calibration coefficients were provided by Tahnk et al. 2001a [10], Tahnk et al. 2001b [11], Tahnk et a. 2002 [12]. Six et al. 2004 [13] focused on Dome-C to construct an empirical bidirectional reflectance distribution function (BRDF) designed to monitor the degradation of the Satellite Pour l'Observation de la Terre (SPOT)-4 land use sensor. During the mid 2000's, Dome-C surface based multi-spectral measurements, where used to model the BRDF over the site [14][15][16][17]. It was also discovered that snow grain size and shape influence the spectral reflectance especially for near infrared (NIR) and shortwave infrared (SWIR) wavelengths, which can change seasonally due to snow metamorphosis [18][19][20][21]. Soon thereafter, Dome-C was established to monitor the stability of sensors with onboard calibration systems sensors such as MODIS and to compare to their relative L1B reflectance differences

[22][23][24][25]. Dome-C along with other invariant targets and intercalibration methods was used to provide a consistent multiple overlapping AVHRR calibrated sensor [26][27][28]. Dome-C is a Committee on Earth Observation Satellites (CEOS) recommended cal/val site and is widely used to monitor sensor performance and to compare sensor calibration differences [29].

Dome-C is a French-Italian scientific station directed by the French Polar Institute and the Italian polar institute and is positioned on the East Antarctic plateau at 75.1° South and 123.4° East. Polar orbiting sun-synchronous satellite cross-track sensors observe Dome-C multiple times a day [22]. The polar latitudes limit the Dome-C solar illumination between the southern hemisphere spring and fall equinox with the lowest observed solar zenith angles occurring during summer solstice. The permanent snow-covered Antarctic plateau has a high surface reflectance for wavelengths less than 1 μm. The Dome-C high surface elevation of 3200 m and long distance (1000 km) from the nearest coast limits the cloud cover, snow accumulation, and aerosol coverage. The site has very low water vapor burden due to the cold air temperature that remains below freezing year-round. The cold temperatures also limit the seasonal snow metamorphosis over summer. The low wind speeds over the flat surface create a spatially homogeneous surface with low surface roughness due to the relatively small scale sastrugi compared with the rest of Antarctica [13][24].

The objective of this study is to further characterize the Dome-C invariant target by correlating real-time auxiliary data with the observed Dome-C reflectances. Section 2 describes the Dome-C invariant target method, which considers snow metamorphosis, the Terra and Aqua MODIS observed Dome-C spurious inter-annual reflectance outliers and compares the Dome-C spectra against the DCC and Libya-4 spectra to reveal any wavelength dependent differences. Section 3 analyzes the Dome-C reflectances for any correlation with the Antarctic Oscillation index, broadband surface albedo, and ozone concentration. The seasonal and inter-annual ozone concentration variability is described to optimally correlate the ozone concentration with Dome-C reflectance to determine ozone correction factors. These corrections factors are then used to reduce the Dome-C MODIS trend uncertainty. Section 4 contains the conclusions.

2. METHODOLOGY

2.1 Data

The Terra and Aqua MODIS Collection 6.1 L1B radiances used in this study were downloaded from the Atmospheric Science Data Center (ASDC) at NASA Langley Research Center. The monthly Antarctic Oscillation (AAO) indices are obtained from the NOAA AAO web site [30][31]. The monthly column ozone over Dome-C derived from the CERES SYN1deg-month product [3] was downloaded from the CERES ordering, subsetting, and ordering tool [32]. The CERES SYN1deg product utilizes the Goddard Space Flight Center (GSFC) Global Modelling and Assimilation Office (GMAO) Goddard Earth Observing System (GEOS) 5.4.1 reanalysis product [33] column ozone, which is a combination of TOMS, Aura-OMI and NPP-OMPS retrievals. The Baseline Surface Radiation Network (BSRN) [34] Dome-C [35] surface and 32-m tower radiometer minute resolution fluxes were used to compute the monthly surface broadband albedo. The Dome-C, Libya-4, and precise-DCC SCIAMACHY Earth scene spectral were obtained from the NASA-Langley SCIAMACHY spectral plotting tool [36] [37][38].

2.2 The Dome-C invariant target methodology

The CERES project Dome-C invariant target methodology averages the instantaneous MODIS pixel-level near nadir (<10° view angle) radiances that are located over the Dome-C region of interest (0.6°x0.6° region centered at 75.1° South latitude and 123.4° East longitude). If the instantaneous pixel radiance standard deviation or homogeneity within the ROI is less than 1.5%, the measurement is identified as a clear-sky observation. This study presents analysis for MODIS band 1 (0.645 μm), band 2 (0.86 μm), band 3 (0.48 μm) and band 4 (0.55 μm). The Hudson et al. 2006 [16] parameterized snow BRDF is reduced to a second order fit with respect to cosine solar zenith angle for near nadir measurements [22][25]. We found no significant difference between a second order and linear. The first 5-years of the MODIS record is used to construct the TOA radiance as a function of cosine solar zenith angle model referred to as a directional model in this study. Nakamura et al. 2001 [19] has shown that as snow ages, otherwise known as snow metamorphosis, the surface to volume ratio decreases and the effective snow grain size increases. The surface albedo has been shown to vary seasonally over Antarctica due to snow metamorphosis [21][39]. However, precipitation can inhibit snow metamorphosis [40]. Here, snow metamorphosis was considered by computing pre-solstice and post-solstice directional models for each MODIS channel. The Rayleigh scattering for a surface albedo of 0.8 is twice as large as for a surface albedo of 0.0 [14]. The Vostock and South Pole station observed ~ 0.97 surface albedo was uniform across the

UV and visible wavelengths. The surface albedo for NIR and SWIR wavelengths is dependent on snow grain size and rapidly decreases to 0.15 at 1.5µm [41].

As expected, there is no pre-solstice and post-solstice difference in the directional model linear regression coefficients for the 0.46-µm Terra-MODIS channel (Fig. 2a). The 0.46-µm channel is not impacted by snow grain size and has a strong Rayleigh scattering component. Unlike the 0.46-µm, the 0.86-µm (Fig. 2b) channel shows a clear distinction between pre-solstice and post-solstice directional models. The two directional models converge during solstice solar conditions. This channel is dependent on snow grain size and shows the seasonal impact of snow metamorphosis as the Dome-C summer ensues. Like the 0.46-µm channel, both the 0.55-µm and 0.65-µm channel pre- and post-solstice directional models do not show any significant differences (not shown).

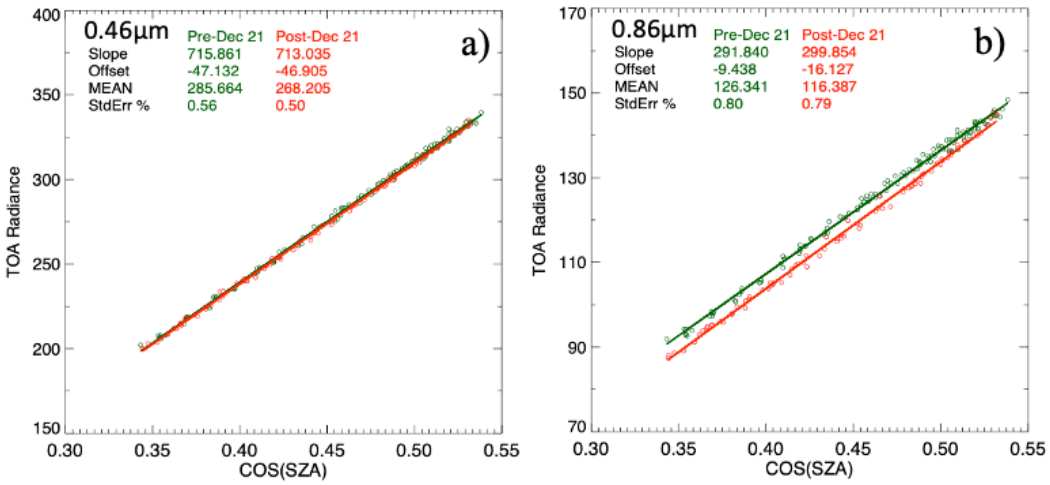

Fig. 2. The Terra-MODIS (**a**) 0.46-µm and (**b**) 0.86-µm channel Dome-C pre-solstice (green points and line) and post-solstice (red points and line) directional models (TOA radiance vs cosine solar zenith angle) based on the first 5 years of data. The linear regression slope, offset and standard error as well as the mean radiance values are given in the upper left of the plot. TOA radiance units are in $Wm^{-2}sr^{-1}\mu m^{-1}$.

2.3 Dome-C TOA response natural variability

To determine the Dome-C natural variability, we compare the Dome-C TOA response timeseries with those from the DCC and Libya-4 invariant targets over the Terra and Aqua-MODIS records. The DCC invariant target approach collectively tracks DCC-identified pixels [42][43][27]. Tropical DCC are near-Lambertian and spectrally flat for wavelengths less than 1 µm, and solar and view angle conditions less than 40°. The bright DCC tropopause targets greatly limit the water vapor absorption. The Libya-4 Saharan Desert site is also a CEOS recommend invariant target. The Libya-4 invariant target approach is similar to the Dome-C approach [43][27]. Directional models are empirically derived using the first 5 years of MODIS near nadir observations. The variation in cosine solar zenith angle not only considers the surface reflectance but also the seasonal atmospheric conditions. All invariant target TOA reflectances have seasonal dependencies, however, the interannual variability of these targets are small compared to the seasonal dependencies. The sun-synchronous angular, seasonal, and local time observations are repeated annually and ensure that these dependencies are not aliased into the invariant target inter-annual variability.

Fig. 3a and 3b show the Aqua and Terra-MODIS band 3 (0.46 µm) TOA response over the three invariant targets. For the 0.46-µm channel no invariant target outliers were observed. The invariant targets clearly show that Terra-MODIS radiometric noise is greater than for Aqua-MODIS. All three invariant target Terra-MODIS reflectances show an increase in the TOA response during 2013. The Terra-MODIS 0.46-µm channel has unresolved polarization and response versus scan angle dependencies [44]. The Libya-4 TOA response shows a distinct coinciding Terra and Aqua MODIS 0.55-µm, 0.65-µm and 0.86-µm channel anomaly during 2013. Whereas the Dome-C MODIS 0.55-µm and 0.65-µm channel response, shows a positive and negative anomaly during the austral summer of 2015-2016 and 2019-2020, respectively. The next section will compare the invariant target spectral response for any wavelength dependent mechanisms.

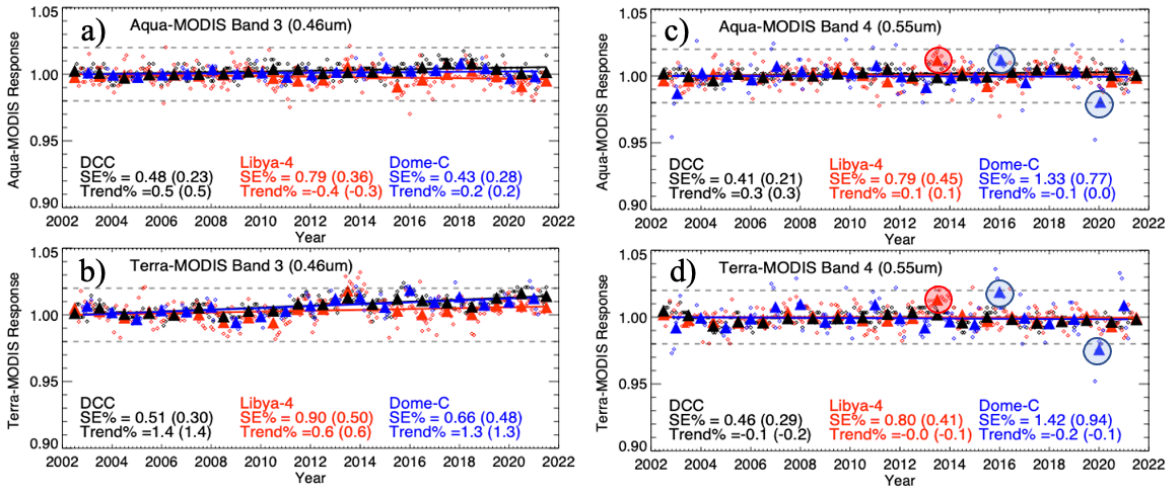

Fig. 3. The Aqua (**a**) and Terra (**b**) MODIS 0.46-µm channel and the Aqua (**c**) and Terra (**d**) MODIS 0.55-µm channel DCC (red), Libya-4 (red), and Dome-C (blue) normalized TOA monthly (small open circles) and annual (solid triangles) response. The temporal linear regression standard error (SE%) and trend slope (Trend%) over the record for each invariant target is given at the bottom of the plot. The monthly statistics are shown on the left and the annual statistics on the right in parenthesis. The thin black dashed line represents a ±2% change in calibration from the thin solid black line representing perfect stability. The red shaded circles identify the Libya-4 response anomaly during 2013, whereas the blue shaded circles denote the austral summer 2015-2016 and 2019-2020 Dome-C anomalies. Note the Terra-MODIS 0.46µm (Fig. 3b) calibration drift during 2013 where all three invariant targets show an anomaly.

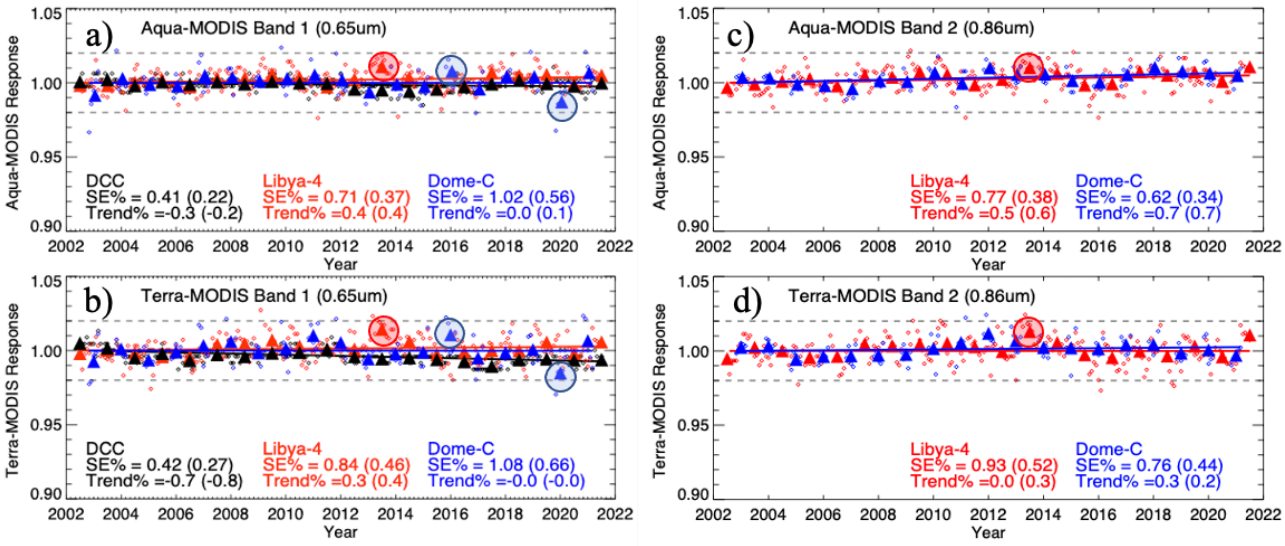

Fig. 4. Same as Fig. 3 except for the Aqua (**a**) and Terra (**b**) MODIS 0.65-µm channel and the Aqua (**c**) and Terra (**d**) MODIS 0.86-µm channel TOA response.

2.4 Dome-C, DCC, Libya-4 SCIAMACHY spectra

Figure 5 shows the Dome-C, DCC and Libya-4 SCIAMACHY mean observed spectra. The Dome-C and DCC spectra are very similar for wavelengths less than 1 µm. The Dome-C snow grains and DCC ice crystals have similar reflectance behaviors. A few wavelength-dependent differences can be explained. Dome-C is a bit brighter over the 0.48-µm spectral range. Both Dome-C and DCC have bright surfaces, however, the Dome-C surface is located at a much lower elevation and has greater Rayleigh scattering than DCC. The Dome-C 0.55-µm and 0.65-µm reflectance is slightly darker than DCC. This is due to the increased ozone concentration over the poles than observed over tropical DCC. The Dome-C 0.86-µm reflectance is slightly darker than DCC, because the snow grain size is larger than the DCC ice

crystals, which are suspended in the atmosphere. The Libya-4 TOA spectral reflectance is not correlated with either the DCC or Dome-C reflectance. The Libya-4 TOA reflectance increases as the wavelength increases after disregarding the near UV Rayleigh scattering, whereas the Dome-C and DCC TOA reflectance mostly decreases as wavelength increases. Libya-4 does not seem to be impacted by ozone absorption as the other two invariant targets.

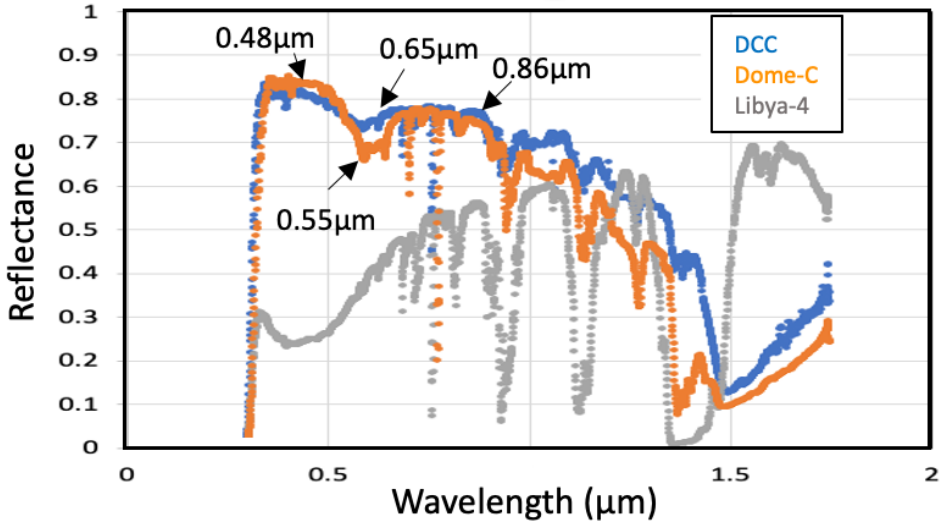

Fig. 5. The DCC (blue), Dome-C (orange) and Libya-4 (gray) SCIAMACHY mean spectra observed between 2002 and 2010.

3. RESULTS

3.1 Dome-C TOA reflectance comparison with AAO, surface albedo, and ozone concentration

The Antarctic Oscillation (AAO) or Southern Annular Mode describes the intensity and migration of the Southern Ocean westerlies. During a positive AAO, the circumpolar westerlies intensify and migrate towards Antarctica. During a negative AAO, the westerlies weaken and move towards Australia. The AAO is a low frequency event that tends to last about two weeks. The timing between positive and negative events is random and range from a week to a few months [45]. Lubin et al. 2005 [46] suggests that positive AAO events decreases the probability of Dome-C cloud cover and snowfall. Arblaster et al. 2006 [47] study suggests that ozone concentration may be a driver of the AAO variability. Fig. 6b shows that for the austral summer of 2015 and 2016 there was a positive AAO event and for the 2019-2020 summer there was a negative event.

Fig. 6a shows the broadband surface albedo deseasonalized anomalies based on Dome-C BSRN ground and tower irradiance measurements. Observed shortwave irradiances are averaged to daily averages in the following manner. One minute data are averaged to 15 minutes requiring a minimum of 7 minutes to have a valid average. We then fill some data gaps by converting downward irradiances to transmission and linearly interpolating across gaps of four hours or less. The 15-minute data are averaged to hourly values and then hourly averages are integrated across the day, weighted by cosine of the solar zenith angle. The daily upwelling and downwelling fluxes were averaged monthly and the ratio of the upwelling and downwelling flux denotes the albedo. Only the months of November through February are plotted. No BSRN measurements are available at Dome C before 2010. There seems to be a downward trend from 2010 and ending in 2016, after which the albedo anomalies were noisy. Comparing the surface albedo anomaly with the AAO index, shows that for the austral summer of 2105 and 2016 the surface albedo anomaly was negative and the AAO index was positive, while for 2019 and 2020, shows the opposite, where the AAO and surface albedo anomaly was negative before the solstice.

Figure 6c shows the ozone concentration anomaly. The ozone anomaly behavior is characterized by occasional spikes over the record. The strong ozone positive spike is correlated with the 2019-2020 decrease in the MODIS channel 0.55 µm response. An increase in ozone would increase the solar absorption and thus decrease the solar reflectance to space. Two strong ozone negative spikes are correlated with the 2015-2016 and 2020-2021 austral summer increase in the 0.55-

μm response. A decrease in ozone would decrease the solar absorption allowing more reflection to space. The gray rectangles in Fig. 6 show that the occasional strong ozone concentration anomalies are well correlated with the TOA 0.55-μm reflectance departures. In the next section, we describe the monthly ozone variability over Dome-C in order to find an optimal ozone-based reflectance correction approach.

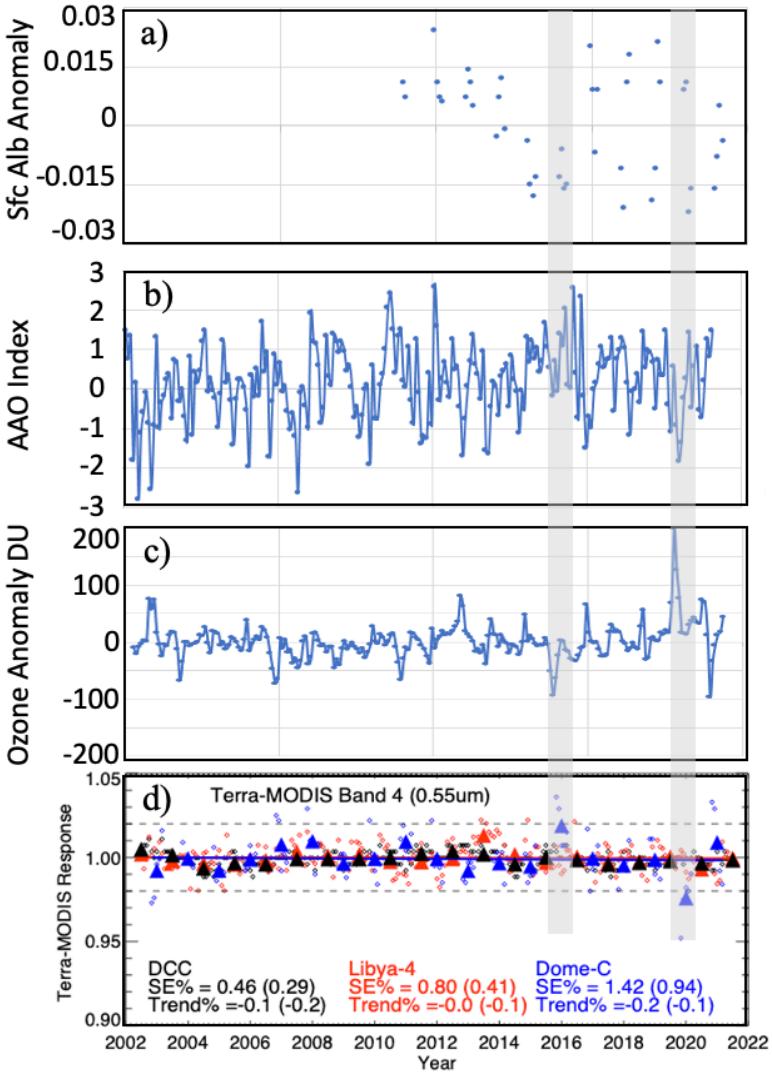

Fig. 6a. The Dome-C monthly (**a**) surface albedo deseasonalized anomaly (unitless), (**b**) Antarctic Oscillation (AAO) index, (**c**) ozone column anomaly (DU) and (**d**) Terra-MODIS TOA response (same as Fig. **3d**). The mean surface albedo was 0.811 and ozone column was 280 DU. The gray rectangles represent the austral summer 2015-2016 and 2019-2020 anomaly period. Note the strong correlation with ozone and weak correlation with surface albedo anomaly and AAO index.

3.2 Dome-C ozone seasonal and interannual variability

Figure 7 illustrates the Dome-C ozone seasonal and interannual variability. During the Antarctic Spring, the ozone hole forms, which is delineated by the low ozone concentrations in Figure 7. The Antarctic ozone hole is formed when the chlorine and bromine contained within the cold polar vortex stratospheric clouds and solar radiation cause ozone depleting reactions [48]. A large anomalous ozone hole formed during the austral Spring of 2015. The ozone hole appeared in early, mid, and late austral Spring in 2016, 2018, and 2020, respectively. A small anomalous ozone hole occurred in 2019 and is surrounding by large ozone concentrations. The post-solstice ozone variations, which range from 260 and 320 DU, are much smaller than the pre-solstice variations, which can range from 100 to 500 DU. The monthly ozone concentrations seem to be well-correlated with the Dome-C TOA reflectance (Fig. 6d). Note the ~0.95 monthly

mean 0.55-µm reflectance value in late 2019 and the two ~1.03 monthly mean 0.55-µm reflectance values in late 2015 and 2020. The Dome-C ozone inter-annual variation has the potential of causing an 8% TOA 0.55-µm reflectance variation. The Dome-C monthly 0.55-µm band response trend standard error is ~1% greater than the DCC response. By regressing the ozone concentration with the TOA reflectance and applying the ozone regression coefficients should reduce the Dome-C trend standard error.

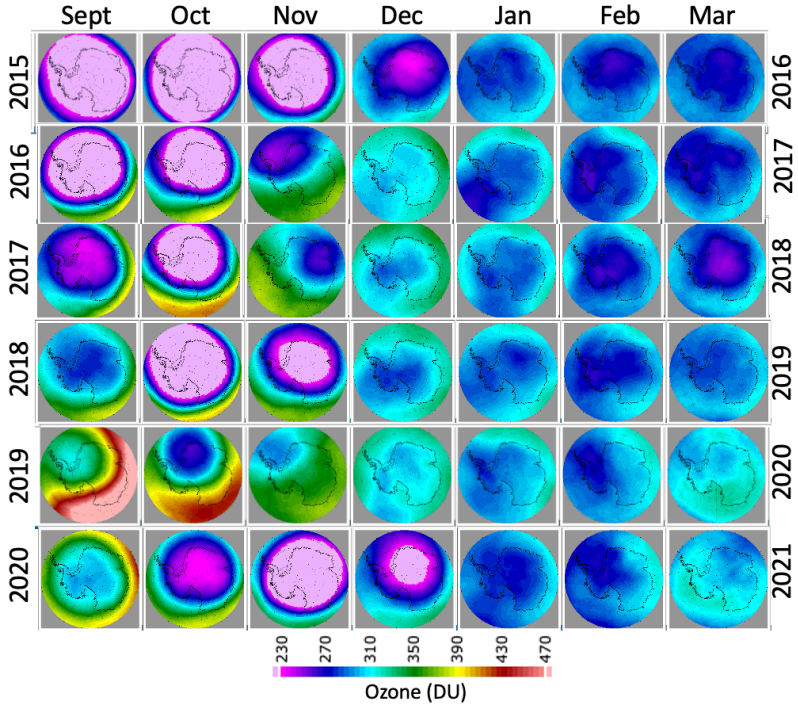

Fig. 7. The 2015 to 2021 September through March monthly mean regional ozone column (DU) centered at the South Pole overlaid with the Antarctic coastline. Greenwich, 90° West, Dateline, and 90° East longitude are oriented towards to the top, left, bottom, and right of the plot. Dome-C is located in the lower right quadrant at 75.1° South and 123.4° East. Note the large ozone variability prior to solstice and low ozone variability following solstice. An anomalous large ozone hole is observed during the austral Spring of 2015, whereas an anomalous small ozone hole is observed during the austral Spring of 2019.

3.3 Dome-C ozone correction

The monthly mean ozone column and the reflectance adjusted for nadir solar conditions based on the directional model are linearly regressed to obtain the ozone correction coefficients. Figure 8 reveal the nearly identical Terra and Aqua-MODIS 0.55-µm channel ozone correction coefficients, which suggests that the correction is robust. The ozone absorption is greater for the 0.55-µm band than the 0.65-µm band, and therefore, the regression slopes (~ -3.0) for the 0.55-µm channel are steeper than those (~ -2.5) for the 0.65-µm channel (not shown). The linear regression standard errors are comprabable. The 0.46-µm and 0.86-µm bands are not significantly correlated with ozone, because the Chappuis ozone bands do not encompass these wavelengths. The cluster of points centered at 280 DU more than likely denote the post-solstice months. Ozone absorption does not explain all of the TOA variability in Fig. 8a. The plot also reveals that the ozone outlier events are not that common. Some Dome-C invariant target approaches do not take into account the ozone absorption because the large ozone anomalies are infrequent [22][25][27].

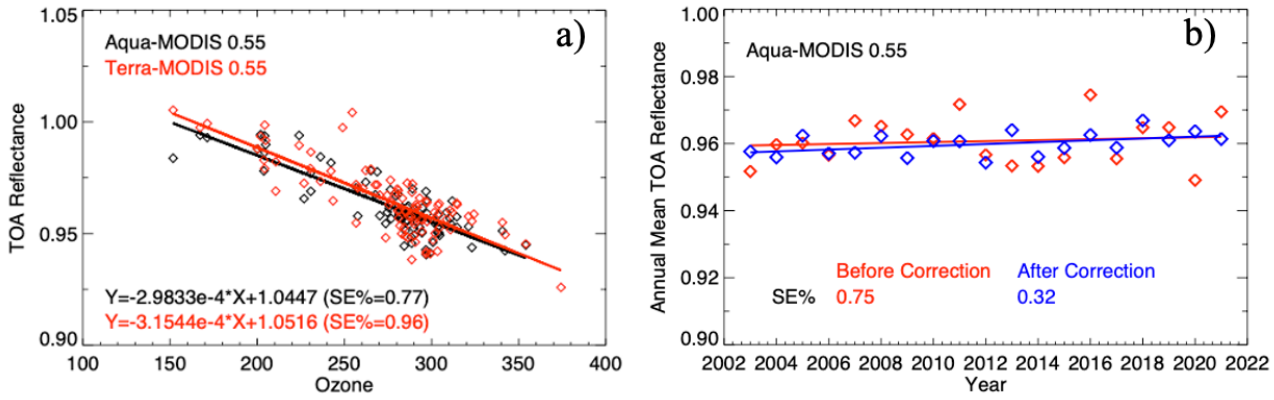

Fig. 8. The monthly TOA reflectance adjusted for nadir sun conditions as a function of the ozone column in DU units for the Aqua (black open circles) and Terra (red open circles) -MODIS (**a**) 0.55-µm and (**b**) 0.65-µm channels. The linear regression slope, offset, and standard error (SE%) are located at the bottom of the plot

The ozone correction coefficients are applied to the TOA radiances and the directional models are recomputed for the Terra-MODIS 0.55-µm channel. Figure 9 shows that the directional model trend standard error was reduced from 1.90% to 1.25% for pre-solstice conditions after ozone correction. However, the post-solstice directional model standard error remains the same as expected. The post-solstice directional model standard error is close to that of the 0.86-µm diectional model standard error of 0.79 (Fig. 2b). However, the pre-solstice 0.55-µm ozone corrected standard error of 1.25% (Fig. 9b) is larger than the 0.86-µm standard error of 0.80% (Fig. 2b). This would suggest that the monthly mean ozone concentration is perhaps temporally too coarse to resolve the daily ozone variability or that the GEOS reanlysis product stratospheric ozone advection and gradients are not well modeled. The Dome-C TOA instantaneous observed reflectances are corrected for ozone absorption after which the ozone adjusted directional models are applied. The Aqua-MODIS before and after ozone corrected trends based on the annual mean Dome-C reflectances are shown in Fig. 8b. The Aqua and Terra-MODIS 0.55-µm and 0.65-µm trend standard errors were reduced by half (Table 1). The Aqua-MODIS 0.55-µm and 0.65-µm ozone corrected Dome-C reflectance trend standard errors are on par with their 0.46-µm and 0.86-µm counterparts.

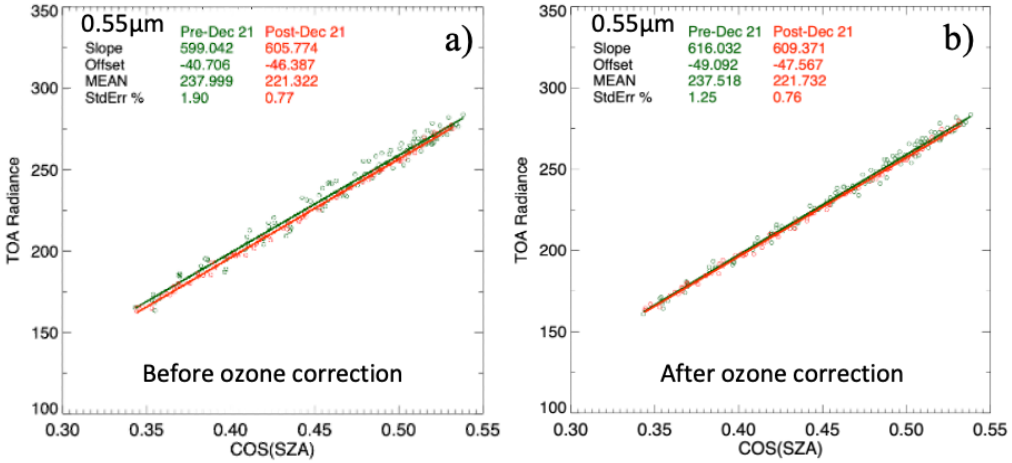

Fig. 9a. Same as Fig. 2 except the Terra-MODIS 0.55-µm channel (**a**) before ozone correction and (**b**) after ozone correction based on the Fig. 8a coefficients. Note the pre-solstice TOA reflectance scatter is reduced after applying the ozone correction coefficients.

Table 1. The linear trend standard error (%) of the annually averaged Dome-C Aqua- and Terra-MODIS reflectances before in () and after ozone correction. Note that the 0.46-µm and 0.86-µm are not impacted by ozone.

Dome-C	0.46µm	0.55µm	0.65µm	0.86µm
Aqua	0.28	(0.77) 0.32	(0.56) 0.36	0.34
Terra	0.48	(0.94) 0.42	(0.66) 0.30	0.44

4. CONCLUSIONS AND FUTURE WORK

Dome-C is a recommended CEOS invariant target, which has been extensively used by the calibration community for monitoring onboard calibration systems and inter-calibration of the sun-synchronous polar orbiting sensors. Dome-C is a high-altitude calibration target located on the East Antarctic interior plateau, which has a permanent bright, flat, and homogeneous snow-covered surface with little aerosol, cloud cover, snowfall, and water vapor burden. Dome-C's near polar location guarantees it is observed multiple times a day by polar orbiting sensors. The Dome-C BRDF corrections were characterized by a radiance versus cosine solar zenith angle linear regression referred to as a directional model. The 0.86-µm channel Dome-C reflectance decreased over the summer due to snow metamorphosis. As snow ages over the summer the snow grain size increases. Pre-solstice and post-solstice directional models were computed to account for snow metamorphosis. The 0.46-µm, 0.55-µm and 0.65-µm channels were not impacted by snow metamorphosis. Both the Terra and Aqua MODIS Dome-C visible reflectance showed coinciding occasional inter-annual anomalies when compared against DCC and Libya-4 invariant target observations. The objective of this study was to determine if the Dome-C reflectances can be further characterized with near real-time auxiliary observations to remove the occasional interannual anomaly.

The Dome-C reflectances were evaluated for any relationship with the Dome-C surface broadband albedo, AAO index, and ozone concentration values. A strong relationship with total column ozone was observed for the 0.55-µm and 0.65-µm MODIS channels. The Chappuis ozone absorption band encompasses the 0.55-µm and 0.65-µm channels but does extend to the 0.48-µm and 0.86-µm channels. The areal extent of the ozone concentration varied greatly inter-annually prior to the solstice, whereas the post-solstice ozone variability was found to be nearly constant. The monthly Dome-C reflectances were linearly regressed with ozone to derive the ozone correction coefficients. The coefficients were applied to the 0.55-µm and 0.65-µm directional models. The standard error of the pre-solstice directional was reduced from 1.90% to 1.25% while the post-solstice directional model standard error had an unchanged value of 0.76%. The Aqua- and Terra-MODIS Dome-C ozone corrected trend standard errors were reduced by half for both the 0.55-µm and 0.65-µm channels, and were similar to the 0.46-µm and 0.86-µm trend standard errors.

ACKNOWLEDGEMENTS

This research has been supported by the NASA CERES project.

REFERENCES

[1] Wielicki, B. A., B. R. Barkstrom, E. F. Harrison, R. B. Lee III, G. L. Smith, and J. E. Cooper, "Clouds and the Earth's Radiant Energy System (CERES): An Earth Observing System experiment," *Bull. Amer. Meteor. Soc.* 77, 853–868 (1996)

[2] Loeb, Norman G.; Doelling, David R.; Wang, Hailan; Su, Wenying; Nguyen, Cathy; Corbett, Joseph G.; Liang, Lusheng; Mitrescu, Cristian; Rose, Fred G.; Kato, Seiji (2018) Clouds and the Earth's Radiant Energy System (CERES) Energy Balanced and Filled (EBAF) Top-of-Atmosphere (TOA) Edition 4.0 Data Product, *Journal of Climate*, 31, 895-918, https://doi.org/10.1175/JCLI-D-17-0208.1

[3] Doelling, D., N. Loeb, D. Keyes, M. Nordeen, D. Morstad, C. Nguyen, B. Wielicki, D. Young, and M. Sun, 2013b: Geostationary Enhanced Temporal Interpolation for CERES flux products. *J. Atmos. Oceanic Technol*. Vol. 30, No. 6, June 2013: 1072-1090, doi:10.1175/JTECH-D-12- 00136.1

[4] CHRISTOPHER L. BREST & WILLIAM B. ROSSOW (1992) Radiometric calibration and monitoring of NOAA AVHRR data for ISCCP, International Journal of Remote Sensing, 13:2, 235-273, DOI: 10.1080/01431169208904037
[5] C. R. Nagaraja Rao and J. Chen, "Calibration of the visible and near-infrared channels of the advanced very high resolution radiometer (AVHRR) after launch," Proc. SPIE 1938, 56–66 (1993), http://dx.doi.org/10.1117/12.161571.
[6] C. R. Nagaraja Rao and J. Chen, "Intersatellite calibration linkages for the visible and near-infrared channels of the Advanced Very High Resolution Radiometer onboard the NOAA-7, −9, and −11 spacecraft," Int. J. Remote Sens. 16(11), 1931–1942 (1995), http://dx.doi.org/10.1080/01431169508954530.
[7] Rao, C.R.N., and J. Chen, "Revised post-launch calibration of the visible and near-infrared channels of the Advanced Very High Resolution Radiometer (AVHRR) on the NOAA-14 spacecraft," Int. J. Rem. Sens., 16, 1931-1942 (1999)
[8] Loeb, N. G., 1997: In-flight calibration of NOAA AVHRR visible and near-IR bands over Greenland and Antarctica. Int. J. Remote Sens., 18, 477–490.
[9] Masonis, S. J., and S. G. Warren, 2001: Gain of the AVHRR visible channel as tracked using bidirectional reflectance of Antarctic and Greenland snow. Int. J. Remote Sens., 22, 1495–1520.
[10] Tahnk, W. R., and J. A. Coakley Jr., 2001a: Improved calibration coefficients for NOAA-14 AVHRR visible and near-IR channels. Int. J. Remote Sens., 22, 1269–1283.
[11] Tahnk, W. R., and J. A. Coakley Jr., 2001b: Updated calibration coefficients for NOAA-14 AVHRR channels 1 and 2. Int. J. Remote Sens., 22, 3053–3057.
[12] Tahnk, William R., and James A. Coakley , Jr. " Improved Calibration Coefficients for NOAA-12 and NOAA-15 AVHRR Visible and Near-IR Channels". Journal of Atmospheric and Oceanic Technology 19.11 (2002): 1826-1833, https://doi.org/10.1175/1520-0426(2002)019<1826:ICCFNA>2.0.CO;2
[13] D. Six, M. Fily, S. Alvain, P. Henry, and J.-P. Benoist, "Surface characterization of the Dome Concordia area (Antarctica) as a potential satellite calibration site, usingSpot 4/Vegetation instrument," Rem. Sens. Environ. 89, 83-94 (2004) [doi:10.1016/j.rse.2003.10.006].
[14] R. Pirazzini, "Surface albedo measurements over Antarctic sites in summer," J. Geophys. Res. 109, D20118 (2004) [doi:10.1029/2004JD004617]
[15] Painter, T. H., and J. Dozier (2004), Measurements of the hemispherical-directional reflectance of snow at fine spectral and
angular resolution, J. Geophys. Res., 109, D18115, doi:10.1029/2003JD004458
[16] Hudson, S. R., S. G. Warren, R. E. Brandt, T. C. Grenfell, and D. Six (2006), Spectral bidirectional reflectance of Antarctic snow: Measurements and parameterization, J. Geophys. Res., 111, D18106, doi:10.1029/2006JD007290.
[17] Hudson, S. R., and S. G. Warren (2007), An explanation for the effect of clouds over snow on the top-of-atmosphere bidirectional reflectance, J. Geophys. Res., 112, D19202, doi:10.1029/2007JD008541
[18] Nolin, A.W., & Dozier, J. (2000). A hyperspectral method for remotely sensing the grain size of snow. Remote Sensing of Environment, 74(2), 207−216.
[19] Tsutomu Nakamura, Osamu Abe, Tomohiro Hasegawa,Reina Tamura, Takeshi Ohta, Spectral reflectance of snow with a known grain-size distribution in successive metamorphism, Cold Regions Science and Technology 32 Ž2001. 13–26
[20] Kuipers Munneke, P., C. H. Reijmer, M. R. van den Broeke, G. Ko¨nig-Langlo, P. Stammes, and W. H. Knap (2008), Analysis of clear-sky Antarctic snow albedo using observations and radiative transfer modeling, J. Geophys. Res., 113, D17118, doi:10.1029/2007JD009653
[21] Zhonghai Jin, Thomas P. Charlock, Ping Yang, Yu Xie, Walter Miller, Snow optical properties for different particle shapes with application to snow grain size retrieval and MODIS/CERES radiance comparison over Antarctica, Remote Sensing of Environment, Volume 112, Issue 9, 2008, Pages 3563-3581, ISSN 0034-4257, https://doi.org/10.1016/j.rse.2008.04.011.
[22] X. Xiong, A.Wu, and B. N.Wenny, "Using Dome C for moderate resolution imaging spectroradiometer calibration stability and consistency," J. Appl. Remote Sens. 3(1), 033520 (2009), http://dx.doi.org/10.1117/1.3116663.
[23] Marc Bouvet & Fabrizio Ramoino (2010) Radiometric intercomparison of AATSR, MERIS, and Aqua MODIS over Dome Concordia (Antarctica), Canadian Journal of Remote Sensing, 36:5, 464-473, DOI: 10.5589/m10-081
[24] C. Cao et al., "Establishing the Antarctic Dome C community reference standard site towards consistent measurements from Earth observation satellites," Can. J. Remote Sens. 36(5), 498–513 (2010).

[25] Sirish Uprety, Changyong Cao, "Radiometric and spectral characterization and comparison of the Antarctic Dome C and Sonoran Desert sites for the calibration and validation of visible and near-infrared radiometers," J. Appl. Rem. Sens. 6(1) 063541 (3 July 2012) https://doi.org/10.1117/1.JRS.6.063541
[26] Heidinger, A. K., W. C. Straka III, C. C. Molling, and J. T. Sullivan, 2010: Deriving an inter-sensor consistent calibration for the AVHRRsolar reflectance data record. Int. J. Remote Sens., 31,6493–6517, doi:10.1080/01431161.2010.496472
[27] Bhatt, R., D. R. Doelling, B. R. Scarino, A. Gopalan, C. O. Haney, P. Minnis, and K. Bedka, 2016: A consistent AVHRR visible calibration record based onmultiple methods applicable for the NOAA degrading orbits. Part I: Methodology. J. Atmos. Oceanic Technol., 33, 2499–2515, doi:10.1175/JTECH-D-16-0044.1
[28] Doelling, D.R., R. Bhatt, B. R. Scarino, A. Gopalan, C. O. Haney, P. Minnis, and K. M. Bedka, 2016: A consistent AVHRR visible calibration record based on multiple methods applicable for the NOAAdegrading orbits. Part II:Validation. J. Atmos. Oceanic Technol., 33, 2517–2534, doi:10.1175/JTECH-D-16-0042.1
[29] G. Chander, T. J. Hewison, N. Fox, X. Wu, X. Xiong and W. J. Blackwell, "Overview of Intercalibration of Satellite Instruments," in *IEEE Transactions on Geoscience and Remote Sensing*, vol. 51, no. 3, pp. 1056-1080, March 2013, doi: 10.1109/TGRS.2012.2228654
[30] https://www.cpc.ncep.noaa.gov/products/precip/CWlink/daily_ao_index/aao/monthly.aao.index.b79.current.ascii (NOAA AAO index)
[31] Mo, K. C., 2000: Relationships between Low-Frequency Variability in the Southern Hemisphere and Sea Surface Temperature Anomalies. *J. Climate*, **13**, 3599-3610.
[32] https://ceres-tool.larc.nasa.gov/ord-tool/jsp/SYN1degEd41Selection.jsp (CERES SYN1deg product)
[33] Rienecker, M. M., and Coauthors, 2008: The GOES-5 Data Assimilation System—Documentation of versions 5.0.1, 5.1.0, and 5.2.0. NASA Tech. Rep. Series on Global Modeling and Data Assimilation, Vol. 27, NASA/TM-2008-105606, 97 pphttps://gmao.gsfc.nasa.gov/
[34] Ohmura, A., Dutton, E. G., Forgan, B., Fröhlich, C., Gilgen, H., Hegner, H., Heimo, A., König-Langlo, G., McArthur, B., Müller, G., Philipona, R., Pinker, R., Whitlock, C. H., Dehne, K., & Wild, M. (1998). Baseline Surface Radiation Network (BSRN/WCRP): New Precision Radiometry for Climate Research, Bulletin of the American Meteorological Society, 79(10), 2115-2136. https://doi.org/10.1175/1520-0477(1998)079<2115:BSRNBW>2.0.CO;2
[35] https://bsrn.awi.de/products/quality-code/physically-possible-limits/dome-c-dom/ (Dome-C BSRN)
[36] https://cloudsway2.larc.nasa.gov/cgi-bin/site/showdoc?mnemonic=SCIAMACHY-SPECTRA-ENHANCED (NASA-Langley SCIAMACHY spectral plotting web tool)
[37] B. R. Scarino, D. R. Doelling, P. Minnis, A. Gopalan, T. Chee, R. Bhatt, C. Lukashin, and C. O. Haney, "A web-based tool for calculating spectral band difference adjustment factors derived from SCIAMACHY hyperspectral data," IEEE Trans. Geosci. Remote Sens., vol. 54, no. 5, pp. 2529-2542, 2016.
[38] H. Bovensmann, J. P. Burrows, M. Buchwitz, J. Frerick, S. Noël, V. V. Rozanov, K. V. Chance, and A. P. H. Goede, "SCIAMACHY: Mission objectives and measurement modes," J. Atmos. Sci., vol. 56, no. 2, pp. 127-150, Jan. 1999.
[39] Wang, X., and C. S. Zender (2011), Arctic and Antarctic diurnal and seasonal variations of snow albedo from multiyear Baseline Surface Radiation Network measurements, J. Geophys. Res., 116, F03008, doi:10.1029/2010JF001864
[40] Picard, G., Domine, F., Krinner, G. *et al.* Inhibition of the positive snow-albedo feedback by precipitation in interior Antarctica. *Nature Clim Change* **2,** 795–798 (2012). https://doi.org/10.1038/nclimate1590
[41] Grenfell, T. C., Warren, S. G., and Mullen, P. C. (1994), Reflection of solar radiation by the Antarctic snow surface at ultraviolet, visible, and near-infrared wavelengths, *J. Geophys. Res.*, 99(D9), 18669– 18684, doi:10.1029/94JD01484.
[42] Doelling, D. R., D. Morstad, B.R. Scarino, R. Bhatt, and A. Gopalan, 2013, The Characterization of Deep Convective Clouds as an Invariant Calibration Target and as a Visible Calibration Technique, *IEEE Trans. Geosci. Remote Sens.*, Vol 51, No. 3, 1147-1159, 10.1109/TGRS.2012.2225066
[43] Bhatt, R., D. R. Doelling, A. Wu, X. Xiong, B. R. Scarino, C. O. Haney, and A. Gopalan, 2014, "Initial Stability Assessment of S-NPP VIIRS Reflective Solar Band Calibration using Invariant Desert and Deep Convective Cloud Targets," *Remote Sens.* 2014, *6*, 2809-2826; doi:10.3390/rs6042809
[44] R. Bhatt, D.R. Doelling, A. Angal, X. Xiong, C.O.Haney, B.R. Scarino, A. Wu, A. Gopalan, "Response Versus Scan-Angle Assessment of MODIS Reflective Solar Bands in Collection 6.1 Calibration," in *IEEE Transactions on Geoscience and Remote Sensing*, vol. 58, no. 4, pp. 2276-2289, April 2020, doi: 10.1109/TGRS.2019.2946963.

[45] http://www.bom.gov.au/climate/sam/ [Australian BOM understanding SAM web site]
[46] Lubin, D., B. H. Kahn, M. A. Lazzara, P. Rowe, and V. P. Walden (2015), Variability in AIRS-retrieved cloud amount and thermodynamic phase over west versus east Antarctica influenced by the SAM, Geophys. Res. Lett., 42, 1259–1267, doi:10.1002/2014GL062285.
[47] Arblaster, Julie M., and Gerald A. Meehl. " Contributions of External Forcings to Southern Annular Mode Trends". *Journal of Climate* 19.12 (2006): 2896-2905. https://doi.org/10.1175/JCLI3774.1
[48] https://csl.noaa.gov/assessments/ozone/2010/twentyquestions/Q10.pdf [NOAA Scientific Assessment of Ozone Depletion web site]